PHYSICAL REVIEW E **79**, 040901(R) (2009)

Tracking and control of neuronal Hodgkin-Huxley dynamics

Ghanim Ullah[1,*] and Steven J. Schiff[1,2]
[1]*Center for Neural Engineering, Department of Engineering Science and Mechanics, The Pennsylvania State University, 212 Earth-Engineering Sciences Building, University Park, Pennsylvania 16802, USA*
[2]*Departments of Physics and Neurosurgery, The Pennsylvania State University, University Park, Pennsylvania 16802, USA*
(Received 26 August 2008; published 13 April 2009)

Nonlinear ensemble state estimation offers a paradigm-shifting improvement in our ability to observe, predict, and control the state of spiking neuronal systems. We use an ensemble Kalman filter to predict hidden states and future trajectories in the Hodgkin-Huxley equations, reconstruct ion dynamics, control neuronal activity including a strategy for dynamic conductance clamping, and show the feasibility of controlling pathological cellular activity such as seizures.

DOI: 10.1103/PhysRevE.79.040901 PACS number(s): 87.19.lr, 05.45.−a, 87.19.ll

In 1952, Hodgkin and Huxley [1] created a set of equations which modeled the dynamics of ion current flow across the neuronal membrane, which formed the foundation for our understanding of the excitable dynamics of nonlinear action potential wave propagation in neurons [2]. Hodgkin and Huxley (HH) based their formulation on experiments that used voltage clamp, a proportional feedback system that delivered current to the interior of a neuron to maintain the transmembrane potential at a given value [3]. The transient dynamics that resulted from such step changes in membrane potential are reflected in the HH equations. More recently, dynamic clamp techniques have introduced the manipulation of a conductance by adjusting the amount of current injected into a neuron while measuring membrane potential [4].

However, despite the existence of this multivariable ionic model for neuronal spiking, neuronal activity is almost always measured through observing just a single variable such as voltage (or calcium, using optical techniques). Such measurements are always uncertain, due to a combination of noise in neurons and amplifiers, as well as uncertainties in recording equipment such as electrode access resistance and capacitance. The introduction of ensemble [5] or unscented [6,7] Kalman filtering (UKF) has enabled the prospect of efficient state estimation of noisy systems with the degree of nonlinearity present in neurons [8]. UKF has recently been extended to tracking spatiotemporal neuronal networks [9]. These works demonstrated such control theory frameworks only on reduced dynamical models of neurons [8,9]. To our knowledge, no one has applied such model-based control theory to reconstruct the full ionic dynamics of neurons.

We here demonstrate that a nonlinear ensemble Kalman filter framework can assimilate neuronal data from single voltage measurements alone and reconstruct the full HH ionic dynamics. We further demonstrate that such a strategy can reconstruct additional extracellular ionic dynamics, which are critical in defining the stability and pattern formation of neuronal networks [10]. We show the ability to measure nonvoltage variables from which reconstructions of the unobserved voltage dependent variables and parameters can be performed, and also introduce a strategy for dynamic conductance clamping. Lastly, we demonstrate the use of such a framework to control pathological seizure dynamics.

The transmembrane potential V of a single neuron, normalized to zero in the resting state, is modeled with the HH equations [1]:

$$V = e + \frac{1}{C_m}\int_0^T (I_{\mathrm{K}} + I_{\mathrm{Na}} + I_l + I_{\mathrm{stim}})dt,$$

$$I_{\mathrm{K}} = -g_{\mathrm{K}} n^4 (V - V_{\mathrm{K}}), \quad I_{\mathrm{Na}} = -g_{\mathrm{Na}} m^3 h (V - V_{\mathrm{Na}}),$$

$$I_l = -g_l (V - V_l), \quad dq/dt = \alpha_q (1-q) - \beta_q q, \quad q = m,n,h, \quad (1)$$

where e is the V measurement noise, n^4 and m^3h represent gating variables for potassium, I_{K}, and sodium, I_{Na}, currents, and I_l is the leak current. The rate equations for the gating variables are $\alpha_n = (0.1-0.01V)/[\exp(1-0.1V)-1]$, $\beta_n = 0.125\exp(-V/80)$, $\alpha_m = (2.5-0.1V)/[\exp(2.5-0.1V)-1]$, $\beta_m = 4\exp(-V/18)$, $\alpha_h = 0.07\exp(-V/20)$, and $\beta_h = 1/[\exp(3-0.1V)+1]$.

Recently [10], we have shown that extracellular potassium dynamics, $[\mathrm{K}]_o$, can be represented in a model based on I_{K}, activity of the pump exchanging K^+ and Na^+, I_{pump}, diffusion of potassium to the microenvironment, I_{diff}, and glial buffering, I_{glia} [Fig. 1(a)],

$$[\mathrm{K}]_o = e_{\mathrm{K}} + \int_0^T (0.165 I_{\mathrm{K}} - 2\beta I_{\mathrm{pump}} - I_{\mathrm{diff}} - I_{\mathrm{glia}})dt, \quad (2)$$

where e_{K} is the $[\mathrm{K}]_o$ measurement noise, $I_{\mathrm{pump}} = I_{\max}/[1+\exp(8-[\mathrm{K}]_o)]$, $I_{\mathrm{diff}} = \kappa([\mathrm{K}]_o - k_{o,\infty})$, $I_{\mathrm{glia}} = G_{\mathrm{glia}}/\{1+\exp[(18-[\mathrm{K}]_o)/2.5]\}$. The potassium and leak reversal potentials are updated based on the instantaneous $[\mathrm{K}]_o$ using the Nernst equations,

$$V_{\mathrm{K}} = 70 + 26.64\ln([\mathrm{K}]_o/[\mathrm{K}]_i),$$

$$V_l = 70 + 26.64\ln\left(\frac{[\mathrm{K}]_o + 0.085[\mathrm{Na}]_o + 0.1[\mathrm{Cl}]_i}{[\mathrm{K}]_i + 0.085[\mathrm{Na}]_i + 0.1[\mathrm{Cl}]_o}\right). \quad (3)$$

We consider a spherical cell with a radius of 13 μm and parameters given in [22]. We set K^+ in the nearby infinite reservoir (bath solution in a slice preparation, or vasculature in the intact brain) $k_{o,\infty} = 4.0$ mM, and intra- to extracellular volume ratio $\beta = 7$ [11].

The UKF approximates the *a posteriori* probability den-

*ghanim@psu.edu

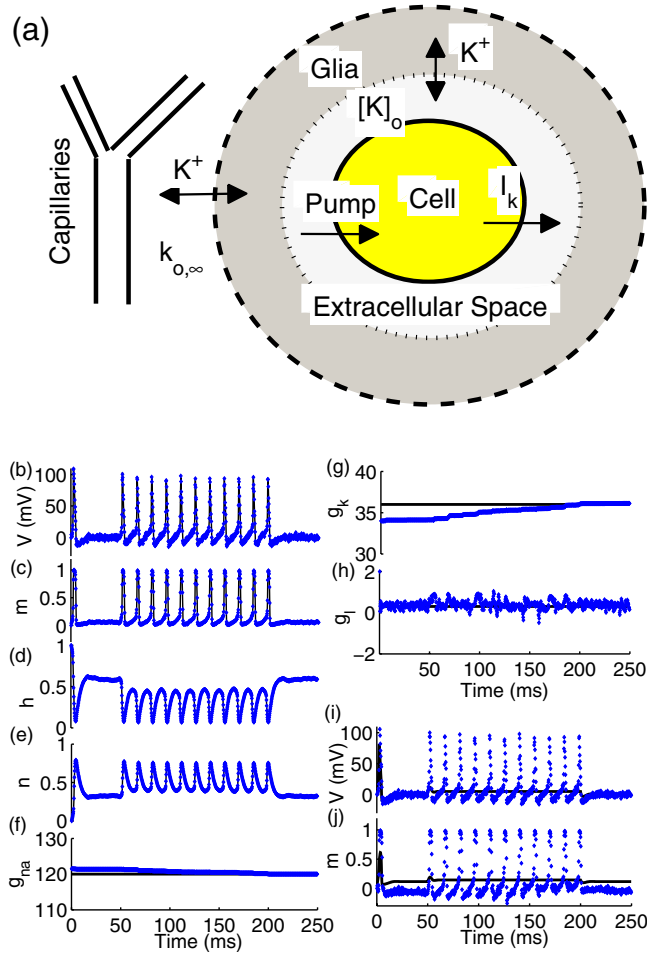

FIG. 1. (Color online) (a) A schematic of the model dynamics: the cell releases K^+ through I_K, which is either pumped back into the cell through K^+-Na^+ exchange pumps or buffered by the glia from the extracellular region. K^+ can also diffuse to the nearby reservoir (capillaries in tissue or bath solution *in vitro*). (b)–(h) Tracking the dynamics of the HH neuron [true values from the model, black, and uncontrolled estimates, dark gray (blue)]. Fixed reversals of −12 and 10.6 mV (relative to 0 mV resting potential), respectively, are used for K^+ and leak currents ($[K]_o$ fixed), and a constant stimulus $I_{\text{stim}}=10\ \mu\text{A/cm}^2$ is applied to the neuron for $50 \leqslant t \leqslant 200$ ms. (b)–(h) respectively, voltage V, Na^+ channel activation m, Na^+ channel inactivation h, K^+ channel activation n, g_{Na}, g_{K}, and g_l. (i),(j) Inaccurate model gives accurate estimates: same as (b),(c) except constant α_m is used [$\alpha_m=0.5$ black, α_m estimated dark gray (blue)]. Noise $e=0.5$, $\sigma=14$.

sity of the estimated state by a Gaussian distribution, and propagates the estimated system state mean and covariance by specifying an ensemble of points that characterize the state variability—*sigma points* (σ). Given a function F describing the dynamics of the system [Eqs. (1)–(3)], and observation function W contaminated by uncertainty characterized by the covariance matrix R, for a D-dimensional estimated state $\bar{x}$ the UKF generates the $2D$ sigma points $X_1,\ldots,X_{2D}$ which are the $2D$ columns of the matrix $\bar{x} \pm \sqrt{DP}$, where P is the estimated covariance matrix of the state x. Increasing the number of sigma points increases accuracy but reduces efficiency [6]. Applying one step of the dynamics F to the sigma points, $\tilde{X}_i=F(X_i)$, and denoting the observations of the new states by $\tilde{Y}_i=W(\tilde{X}_i)$, we define the means $\tilde{x}=(1/2D)\Sigma_{i=1}^{2D}\tilde{X}_i$, $\tilde{y}=(1/2D)\Sigma_{i=1}^{2D}\tilde{Y}_i$, where $\tilde{x}$ and $\tilde{y}$ are the *a priori* state and measurement estimates, respectively. Now define the *a priori* covariances $\tilde{P}_{xx}=(1/2D)\Sigma_{i=1}^{2D}(\tilde{X}_i-\tilde{x})(\tilde{X}_i-\tilde{x})^T$, $\tilde{P}_{xy}=(1/2D)\Sigma_{i=1}^{2D}(\tilde{X}_i-\tilde{x})(\tilde{Y}_i-\tilde{y})^T$, and $\tilde{P}_{yy}=(1/2D)\Sigma_{i=1}^{2D}(\tilde{Y}_i-\tilde{y})(\tilde{Y}_i-\tilde{y})^T$ of the ensemble members. The Kalman filter estimates of the new state and uncertainty are given by the *a posteriori* quantities $\hat{x}=\tilde{x}+K(y-\tilde{y})$ and $\hat{P}_{xx}=\tilde{P}_{xx}-K\tilde{P}_{xy}$, where $K=\tilde{P}_{xy}\tilde{P}_{yy}^{-1}$ is the Kalman gain matrix and y is the actual observation (see [7–9]). Thus $\hat{x}$ and $\hat{P}_{xx}$ are the updated estimated state x and covariance P for the next step. The *a posteriori* estimate of the observation $\hat{y}$ is recovered by $\hat{y}=W(\hat{x})$. Thus, by augmenting the observed state variables with unobserved state variables and system parameters, UKF can estimate and track both unobserved variables and system parameters. Although there are more sophisticated methods to explicitly account for model inadequacy [12], we here minimize model inadequacy by carefully choosing the process noise added to state $\tilde{x}$.

In contrast with recent work on reduced models [8,9], we seek to reconstruct the full HH ionic dynamics using noisy voltage measurements. Conversely, we wish to employ $[K]_o$ measurements to reconstruct voltage and other gating variables and parameters. We want to generate control signals based on the measured and estimated variables while at the same time optimizing the energy requirements.

As a first example we use the original HH model [Eq. (1)] to demonstrate that all variables and parameters can be reconstructed from the measurements of a single variable (Fig. 1). In Fig. 1(b) we show the voltage measurements while the estimated gating variables m, h, and n are shown in Figs. 1(c)–1(e). We also tracked the three current conductances g_{Na}, g_{K}, and g_l in Figs. 1(f)–1(h), respectively.

To illustrate the power of this technique under significant model inadequacy [12], we set α_m constant, and track it as a parameter rather than a function of V (with trivial dynamics as in [8]) in Figs. 1(i) and 1(j). Although this model by itself is incapable of spiking (black traces), when the data from Fig. 1(b) are assimilated, the UKF framework reconstructs spiking sufficiently well to track the dynamics [dark gray (blue) traces]. This α_m tracked by UKF is within 20–30% root mean square (time step dependent) of the full functional form of α_m, and is sufficiently close to enable the generation of spike dynamics. A universal need in neuroscience is to be able to track and control systems with incomplete knowledge of the underlying equations [12].

We next add a variable $[K]_o$ parameter to the HH equations. Thus our function F now consists of Eqs. (1) and (3). In Fig. 2 we show the measured membrane potential (top) and the estimated $[K]_o$ (bottom). The filter does a very good job in tracking this additional parameter. All other gating variables and parameters can be estimated and tracked along with $[K]_o$ (not shown).

We followed the strategy of [9] to estimate a control vector [Fig. 3(a)]. In the left panel we show direct proportional control, where control signal c is generated from the noisy measurement y, which is generated by adding noise e to

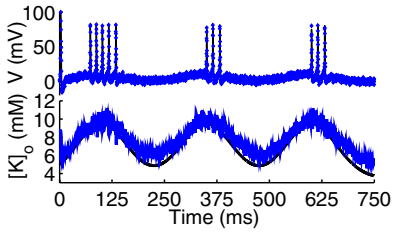

FIG. 2. (Color online) Tracking a variable parameter $[K]_o$ given as $[K]_o = 3.5 + 6\{\exp[-(t-100)^2/2c^2] + \exp[-(t-350)^2/2c^2] + \exp[-(t-600)^2/2c^2]\}$, $c=65$. Measured V (top) and estimated $[K]_o$ (bottom) in dark gray (blue), true values in black. Noise $e=1.0$, $\sigma=16$.

observation variable b following application of observation function W. In the right panel we show Kalman observer control, where the model observer system is used to generate the control vector from the estimated observable $\hat{y}$. In both schemes the control vector is applied to both the system and observer. In Fig. 3(b) we demonstrate use of voltage measurements (top) to control the dynamics of the cell. The extracted Na^+ channel gating variable m is shown in the middle panel. As is clear from the bottom panel, the energy required for the control vector estimation through Kalman observer control is smaller than that used in direct proportional control. In fact, the energy requirements for direct proportional control relative to the energy requirements for Kalman observer control increases exponentially with increased noise in the measurements (inset right bottom), although beyond a certain limit the direct proportional controller becomes unstable (not shown).

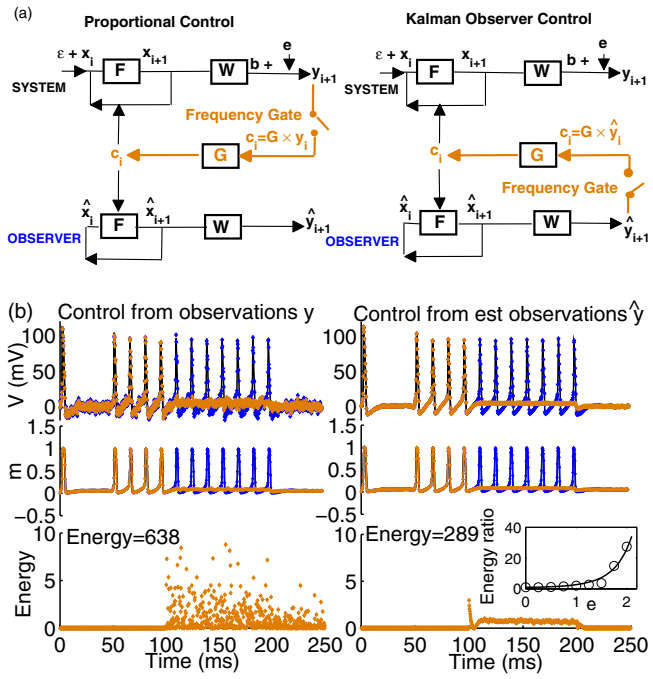

FIG. 3. (Color online) (a) Schematic of Kalman filter observer. System function F acts upon state variable x, and observation function W produces output vector b. Output observable y is generated by adding measurement noise e to b. In the left panel the control signal is constructed directly from actual noisy data by multiplying it with gain G, while in right panel the filter uses the estimated state from the observer. (b) Controlling the dynamics of HH neuron [controlled estimates, light gray (orange); uncontrolled estimates, dark gray (blue); true values, black] using direct proportional (left) and Kalman observer control (right). Panels V, m, and energy used by the controller (sum of squares of control vector). Control vector c is turned on at $t=100$ ms and injected only into V. Inset shows ratio of energy required in direct proportional and Kalman observer control, versus measurement noise (circles), fitted by $\exp(e^{1.7})$. Gain $G=-0.2$, noise $e=1.0$, $\sigma=14$.

Since we can estimate the gating variables and parameters along with $[K]_o$, it is possible to construct control signals based on the estimated gating variables. Such a control framework offers a novel means to modulate neuronal dynamics through various conductances using dynamic clamp [4]. In Fig. 4(a) we show a dynamic clamp simulation where seizure-like activity is controlled through g_K. In previous dynamic clamp methods, the current corresponding to a given ion species, I_i, is calculated in isolation from the relation $I_i = g_i(V-V_i)$, where g_i is the voltage-dependent conductance, and V_i is the reversal potential for an ion species i [4]. In the bottom panel we show $[K]_o$ estimated by the filter. Our state estimation framework has an advantage over this previous methodology in that the current to be injected into the cell to modulate a conductance can be calculated from more complete dynamical descriptions of conductance and gating parameters [from Eqs. (1)–(3)], combined with an optimal strategy for handling model and measurement uncertainty, which, heightened by computational constraints, are major issues in applying dynamic clamp [13].

In Fig. 4(b) we use V measurements to control seizurelike events by applying the control signal to V (top). Such control strategy can be employed experimentally by controlling seizures using an adaptive electric field [14]. Here we place a frequency gate on the filter, tuning the filter such that it applies the control signal only when the frequency of measured or estimated neuronal spiking goes above a certain value (50 Hz). The frequency gate (50 Hz) in the filter allows the controller to modulate only the high-frequency spiking attributed to seizurelike behavior, while allowing the neurons to perform their more normal (low-frequency) functions. This not only minimizes the energy requirements by shutting the controller off when not needed, but can also minimize the long-term damage to brain tissue due to continuous electrical stimulation.

There is considerable evidence relating increased $[K]_o$ to the abnormal patterns of activity during epilepsy and spreading depression [15]. The relatively small extracellular space causes a small I_K to generate moderate changes in $[K]_o$, which enhances the membrane excitability significantly by changing the reversal potentials for K^+ channels. Recent work has explored the bifurcation dynamics of K^+ in single cells and the influence of K^+ on network stability [10].

We therefore reconstruct neuronal dynamics including V based on $[K]_o$ measurements. In the top panel of Fig. 4(c) we show $[K]_o$ measurements, and apply K^+ control at $t=250$ ms. Driving $[K]_o$ to lower levels causes the seizure-like burst firing in V to go to silence (bottom). Controlling seizures with $[K]_o$ has two major advantages: (1) the time scale for $[K]_o$ is slower than the fast dynamics of V and

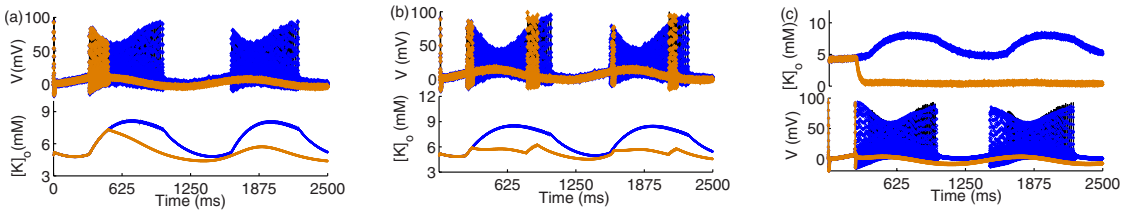

FIG. 4. (Color online) Single cell seizures controlled through g_K (a), V (b), and $[K]_o$ (c). In (a) top panel shows V measurements with [light gray (orange)] and without [dark gray (blue)] control. At $t=500$ ms, g_K is doubled using dynamic conductance clamp, which suppresses the seizure. Bottom panel shows estimated $[K]_o$. In (b) simulation from (a) but control signal is applied to V when the spiking frequency is above 50 Hz. $[K]_o$ is lower after seizures are blocked (bottom panel). In (c) dynamics are generated from, and control signals are applied to, $[K]_o$ measurements. The control vector is injected only into $[K]_o$ (top panel). After injection of control signal V stays close to the resting value (bottom panel). Stimulus $I_{stim}=a\{\exp[(500-t)/2c^2]+\exp[(1750-t)/2c^2]\}$ is applied to the cell, where $a=50$ $\mu A/cm^2$, $c=200$. Gain $G=-0.06$ (a),(b), -0.01 (c); $e=0.5$ (a),(b), $e_k=0.5$ (c). $\sigma=16$.

gating variables, and hence can be more easily implemented in real time, and (2) the $[K]_o$ controller allows us to control the neuronal network rather than a single cell. It has been shown, using ion-selective microelectrodes to measure K^+ activity changes in extracellular space that electrical current could be used to decrease or increase $[K]_o$ [16]. A recent theoretical study [17] predicts a functional block along axons due to K^+ accumulation in the extracellular (submyelinated) space during deep brain stimulation. Recent optical techniques offer the prospect of increasing the speed and decreasing the scale of $[K]_o$ measurements [18].

In conclusion, we have laid the foundation for the framework of model-based data assimilation and control for spiking neuronal systems based on the foundational HH ionic model. This framework has a wide range of potential applications to various systems in biology, where one can use a single measured variable to estimate the variables and parameters that are experimentally inaccessible, and allows us to predict the system trajectory. Examples of similar nonlinearities include the spiking dynamics of heart cells, or the insulin-secreting cells in the pancreas. The prospect of employing our framework in dynamic conductance clamp offers possibilities of addressing the well-known limitations of this technique [4,13]: the need to reconstruct spatial dynamics from point measurements, the need to account for signal transduction analyte concentration changes (such as calcium), and of course the ubiquitous need to account for errors in measurements, modeling, and discrete computation.

This work was supported by NIH Grants No. R01MH50006 and No. K02MH01493, the Pennsylvania Keystone Innovation Zone Program and Tobacco Settlement.

[1] A. L. Hodgkin and A. Huxley, J. Physiol. (London) **117**, 500 (1952).
[2] E. M. Izhikevich, *Dynamical Systems in Neuroscience: The Geometry of Excitability and Bursting* (MIT Press, Cambridge, MA, 2005).
[3] K. S. Cole, *Membranes, Ions and Impulses* (University of California Press, Berkeley, 1972).
[4] J. M. Goaillard and E. Marder, Physiologie **21**, 197 (2006); A. A. Prinz *et al.*, Trends Neurosci. **27**, 218 (2004).
[5] G. Evensen, J. Geophys. Res. **99**, 10143 (1994).
[6] S. J. Julier and J. K. Uhlmann, Proc. SPIE **3068**, 110 (1997).
[7] D. Simon, *Optimal State Estimation* (Wiley-Interscience, New York, 2006).
[8] H. U. Voss and J. Timmer, Int. J. Bifurcation Chaos Appl. Sci. Eng. **14**, 1905 (2004).
[9] S. J. Schiff and T. Sauer, J. Neural Eng. **5**, 1 (2008).
[10] J. Cressman *et al.*, J. Comput. Neurosci. **26**, 159 (2009).; G. Ullah *et al.*, J. Comput. Neurosci. **26**, 171 (2009).
[11] C. J. McBain *et al.*, Science **249**, 674 (1990).
[12] Z. Toth and M. Pena, Physica D **230**, 146 (2007); S. Baek *et al.*, Tellus, Ser. A **58**, 293 (2006).
[13] J. C. Bettencourt *et al.*, J. Neurosci. Methods **169**, 282 (2008); R. J. Butera and M. L. McCarthy, J. Neural Eng. **1**, 187 (2004); I. Raikov *et al.*, J. Neurosci. Methods **132**, 109 (2004).
[14] B. J. Gluckman *et al.*, J. Neurosci. **15**, 590 (2001).
[15] H. Kager *et al.*, J. Comput. Neurosci. **22**, 105 (2007); A. Konnerth *et al.*, Nature **307**, 69 (1984).
[16] A. R. Gardner and C. Nicholson, J. Physiol. (London) **335**, 375 (1983).
[17] S. C. Bellinger *et al.*, J. Neural Eng. **5**, 263 (2008).
[18] V. Montana *et al.*, Biochemistry **28**, 4536 (1989); M. Brasuel *et al.*, Anal. Chem. **73**, 2221 (2001).
[19] M. Bazhenov *et al.*, J. Neurophysiol. **92**, 1116 (2004).
[20] R. S. Fisher *et al.*, Brain Res. **101**, 223 (1976).
[21] E. Scharrer, Q. Rev. Biol. **19**, 308 (1944).
[22] Membrane capacitance $C_m=1$ $\mu F/cm^2$; maximum conductances (mS/cm^2) $g_{Na}=120$, $g_K=36$, $g_l=0.3$; sodium reversal $V_{Na}=115$ mV; ion concentrations (mM) intracellular $[K]_i=130$, extracellular $[Na]_o=130$, intracellular $[Na]_i=20$, extracellular $[Cl]_o=130$, intracellular $[Cl]_i=8$ [19]; maximum pump flux $I_{max}=0.1$ mM/s; and glial buffer strength $G_{glia}=100$ mM/s. Diffusion coefficient of $[K]_o$ to the nearby reservoir κ, from Fick's law, is $\kappa=2D/\Delta x^2=4.0$ s^{-1}, where $D=400\times10^{-6}$ cm^2/s is K^+ diffusion constant in neocortex [20] and $\Delta x\approx15$ μm for brain reflecting average distance between capillaries [21]. The factor 0.165 mM $cm^2/\mu C$ in Eq. (2) converts ionic current to concentration rate of change and is calculated using $\beta A/FV$ [10], where A, V, and F represent cell area, volume, and Faraday constant, respectively.